

Palacký University Olomouc

Faculty of Science

Department of Physical Chemistry



Metal and Metal Oxide Nanoparticles for Catalytic
Applications

Kasibhatta Josena Datta

Summary of doctoral dissertation

Title and Number of the Scientific Field: Chemistry - R12005

Field of Study: Physical Chemistry - 1404V001

Olomouc 2016

The doctoral thesis was prepared under the full-time doctoral program at the Department of Physical Chemistry, Faculty of Science, Palacký University in Olomouc.

Applicant: **Mgr. Kasibhatta Josena Datta**

Supervisor: **Prof. RNDr. Radek Zbořil. PhD.**
Faculty of Science
Palacký University in Olomouc.

Opponents: **Assoc. Prof. Martin Pumera**
Division of Chemistry & Biological Chemistry
School of Physical and Mathematical Sciences
Nanyang Technological University
Singapore.

Prof. Dr. Ing. Miroslav Černík, CSc.
Technical University of Liberec
Department of New Technologies and Applied
Informatics, Liberec.

The standpoint to the doctoral thesis was prepared at the Department of Physical Chemistry, Faculty of Science, Palacký University in Olomouc.

Author's summary was sent on:

The defense takes place on June 23, 2016 before the committee for the defense of the dissertation, field of study Chemistry, No. P1417, Physical Chemistry, No. 1404V001

The dissertation can be found out in the library of the Faculty of Science, Palacký University in Olomouc

.....

Prof. Ing. Pavel Hobza, DrSc.
Chairman of the committee for the defense doctoral thesis

Acknowledgements

First and foremost I wish to express my sincere gratitude to my research supervisor Prof. Radek Zbořil for his generous support, insightful guidance in the last four years, encouragement, cooperation and invaluable suggestions he gave me during the course of this work. I am thankful to him for giving me an opportunity to work under his guidance.

I am thankful to Prof. Michal Otyepka, Head of the Physical Chemistry Department.

I thank my consultant, Dr. M. B. Gawande for his kind support and valuable suggestions and remarks.

I am thankful to Prof. Juan Carlos and Prof. Dunwei Wang for guiding me in various research problems and invaluable discussions during my stay in Institute of Physical Chemistry of the Polish Academy of Sciences, Poland and Department of Chemistry, Boston College.

I would like to thank my collaborators Prof. Varma, Dr. Giorgio, Prof. Yamauchi, Prof. Asefa, Dr. Vasek, Dr. Anuj, Eleni, Dr. Sergi, Dr. Tucek, Dr. Bartak, and Dr. Pechousek.

I am thankful to Dr. Klara, Dr. Claudia, Jana, Petra, Tomanec, Kaslik, and Martin for their constant and timely help with the various characterization techniques.

I would like to thank all my colleagues and batch mates.

I would like to thank administrative staff of RCPTM and Palacký University.

My heartfelt thanks to all my family members for being there for me always. The completion of this dissertation would not have been possible without the support of my husband. You are the pillar of my strength throughout this journey. I would not make it without your unconditional love, understandings and supports. This thesis is a humble offering to my dear husband.

Overview of the author's publications

1. **K. J. Datta**, M. B. Gawande, K. K. R. Datta, V. Ranc, J. Pechousek, M. Krizek, J. Tucek, R. Kale, P. Pospisil, R. S. Varma, T. Asefa, G. Zoppellaro, and R. Zbořil. (2016) 'Micro-mesoporous iron oxides with record efficiency for the decomposition of hydrogen peroxide: morphology driven catalysis for the degradation of organic contaminants'. *J. Mater. Chem. A*, 4, 596-604.
2. **K. J. Datta**, K. K. R. Datta, M. B. Gawande, V. Ranc, K. Čépe, V. Malgras, Y. Yamauchi, R. S. Varma, R. Zbořil. (2016). 'Pd@Pt core-shell nanoparticles with branched dandelion-like morphology as highly efficient catalysts for olefin reduction'. *Chem. Eur. J.*, 22, 1577 – 1581.
3. **K. J. Datta**, A. K. Rathi, M. B. Gawande, V. Ranc, G. Zoppellaro, R. S. Varma, R. Zbořil, Base-free transfer hydrogenation of nitroarenes catalyzed by micro-mesoporous iron oxide, (*ChemCatChem* under revision) (2016)
4. K. K. R. Datta, E. Petala, **K. J. Datta**, J. A. Perman, J. Tucek, P. Bartak, M. Otyepka, G. Zoppellaro, R. Zbořil, NZVI modified magnetic filter paper with high redox and catalytic activities for advanced water treatment technologies. *Chem. Commun.*, 50, 15673-15676 (2014).

Contents

1	Introduction	6
2	Applications of iron oxides	6
3	Experimental section	9
3.1	Materials	9
3.2	Synthesis of the catalysts	9
3.3	Kinetic measurements of H ₂ O ₂ decomposition.....	9
3.4	Catalytic activity of iron oxide in organic pollutant degradation	9
3.5	Characterization techniques.....	10
4	Overview of the main results.....	11
4.1	Micro-mesoporous iron oxide (MMIO) in H ₂ O ₂ decomposition and organic pollutant degradation	11
4.2	MMIO as catalyst for base free transfer hydrogenation of nitroarenes	19
4.3	Porous magnetite prepared from MMIO and used for the reduction of nitroarenes	22
5	Summary.....	27
6	References	28

1. Introduction

Iron oxides are composed of iron and oxygen, which are the most abundant elements on earth. It has a widespread occurrence and can be commonly found in rocks and soils. It is currently an area of intense scientific interest due to a broad variety of promising applications in industry, information storage, medicine, environmental chemistry, geochemistry, soil science *etc.* Furthermore, iron oxides have been extensively studied in diverse fields including catalysis, magnetic storage media and environmental protection.

Altogether, there are sixteen known iron oxides and oxyhydroxides such as α -Fe₂O₃, β -Fe₂O₃, γ -Fe₂O₃, ϵ -Fe₂O₃, FeO and Fe₃O₄ (pure oxides) and α -FeOOH, β -FeOOH, γ -FeOOH, δ -FeOOH, δ' -FeOOH, high-pressure FeOOH, Fe(OH)₃, Fe₅HO₈.4H₂O, Fe(OH)₂ and Fe₁₆O₁₆(OH)_y(SO₄)_z.nH₂O (pure-oxides and oxide-hydroxides). The use of these various oxides and hydroxides are tremendously diverse. The most commonly used iron oxides are hematite (α -Fe₂O₃), maghemite (β -Fe₂O₃) and magnetite (Fe₃O₄). Hematite is paramagnetic, reddish brown, and readily attacked by acids and is the main source of the iron for the steel industry.

Among the various synthetic approaches to prepare iron oxides, thermally induced solid state synthesis are widely exploited, due to its obvious advantages. They are cost-effective, helps to synthesize high yield of products, a range of appropriate precursors for iron oxide synthesis, and possibility to get different iron oxide phases by controlling synthetic variables.

The main aim of the thesis is the morphology controlled preparation of iron oxides (hematite) using thermally induced solid state synthesis (using iron oxalate as the precursor). The as-prepared flower/rod-like iron oxides were further utilized in the environmental applications (hydrogen peroxide decomposition and organic pollutants degradation) and also in catalysis (transfer hydrogenation reaction of nitroarenes using formic acid as the hydrogenating agent). Also, we prepared magnetite by reducing this as-prepared hematite under hydrogen atmosphere and was employed for catalytic reduction of nitroarenes using hydrazine hydrate as the reducing agent under microwave conditions.

2. Applications of iron oxides

The use of iron oxides in human civilization dates back to thousands of years, across all fields, from ancient paintings on walls, to use as pigments for paints and construction industry, as catalyst for industrial syntheses and raw materials for manufacturing. The other applications

include its use as abrasives and polishing agents, sensors, production of photochemicals, adsorbents, flame retardants *etc.* Among all the applications, iron oxides as catalyst gained popular research focus mainly due to their simple and facile synthesis, relatively non-toxic and cost-effective, abundance and eco- friendly nature. Iron oxide catalyst are widely utilized in a large scale in industry, laboratory and environmental processes which includes synthesis of ammonia, high temperature water-gas shift reactions, in organic chemical transformations, Fischer-Tropsch synthesis, PEC water splitting, Fenton reactions, in liquefaction of hydrogen and also it has a potential application in biology and medicine.

Due to its fascinating physical and chemical properties, iron oxide has attracted a great deal of attention in the environmental bioremediation of organic/inorganic pollutants.^{1,2} Toxic organic pollutants in the wastewater represent the most prevalent problem affecting the quality of human life throughout the world.^{3,4} The introduction of novel strategies to generate hydroxyl radical ($\bullet\text{OH}$) is one of the sought-after forefront targets of environmental remediation.⁵ Among all methods, the widely used process for the cleansing of contaminants in water and soils employs Fenton reagent, materials known for their ability to activate the environmentally green-reactant H_2O_2 for the production of $\bullet\text{OH}$.^{6,7} Fenton reagents are composed of ferrous/ferric cations ($\text{Fe}^{2+}/\text{Fe}^{3+}$)⁸⁻¹¹ that activate the catalytic decomposition of H_2O_2 into highly reactive hydroxyl and hydroperoxyl radicals ($\bullet\text{OH}$, $\bullet\text{OOH}$).¹² The $\bullet\text{OH}$ / $\bullet\text{OOH}$ species are potent oxidants (E^0 of 2.31 V and 1.06 V, respectively) with demonstrated efficiency against several organic contaminants. Fenton like reactions that use soluble iron salts (ferric/ferrous) follow the pathway of homogeneous catalysis, they are cost effective and operational easy to device. They show, however, several limitations; of particular note, acid environments and high concentration of metal salts are often necessary in order to support efficiently the catalysis.⁹⁻¹¹ Conversely, large amounts of sludge are produced during the bioremediation process and neutralization of the treated solutions is required, in order to separate the consumed catalyst from the cleansed environment. These limiting factors can be circumvented when a heterogeneous Fenton-like catalyst is used in lieu of the homogeneous catalyst.⁸ Especially, iron oxide-based heterogeneous catalysts constitute a relevant class of earth-abundant materials in terms of its variable efficiencies in H_2O_2 decomposition with rate constants ranging from 10^{-5} to 10^{-2} min^{-1} , depending on the porosity, particles size, crystallinity, and surface area.¹³⁻²¹

Therefore, a considerable research effort has been intensively studied by several groups in recent years on finding synthetic novel routes for nano- or micron-sized iron oxides with porous structures which further helps to increase the efficiency of peroxide activation.^{22,23} Mesoporous iron oxides have been so far synthesized using soft/hard templating methods.²⁴⁻²⁹ However, drawback exists for both approaches leading to a rather poor control of the morphological organization of the iron oxide products, a property that is often compromised during the calcination process. Therefore, it is a difficult task from the synthetic perspective to achieve controlled morphology of iron oxide in a facile and environmental friendly process.

The template free metamorphosis of metal oxalate precursor followed by solid state thermal decomposition of the intermediate product offer a promising strategy to attain a conserved morphology for the synthesis of porous metal oxides.^{30,31} Our earlier studies have shown that the template-free thermally induced solid-state decomposition of iron oxalate precursor can in fact provide such control of the particle structure, size, morphology, surface area and crystallinity, upon changing the reaction conditions and precursor properties.^{15,32-34} In this thesis, we report the generation of such type of iron oxide-based Fenton catalyst, and illustrate a novel approach for the synthesis of morphologically controlled and highly organized micro-mesoporous hematite nanocatalyst, which in turn exhibited the highest rate constant reported to date for hydrogen peroxide decomposition ($1.43 \times 10^{-1} \text{ min}^{-1}$). Furthermore, we describe in detail the material physical/chemical properties, the reasoning behind its high catalytic ability for H_2O_2 activation and extraordinary efficiency in bioremediation processes.

This iron oxide catalyst was further employed for the reduction reaction of nitro compounds. In chemical reactions, catalyst lie at the heart of a multitude of chemical processes. Catalysis is the process in which a small amount material called a catalyst increases the rate of a chemical reaction without itself being consumed. The hydrogenation of nitro compounds is an industrial process which has experienced a revived interest in the past decade due to the innovation of highly selective and eco-friendly solid catalysts. Catalytic transfer hydrogenation (CTH) relies on the *in-situ* formation of atomic hydrogen from hydrogen donors (formic acid, hydrazine hydrate, formates, alcohols *etc.*). The handling of hazardous hydrogen is then avoided and high-pressure equipment is no longer needed. Thus catalytic transfer hydrogenation is of paramount importance and offers safer and greener choice to consider.

3. Experimental section

3.1. Materials: Iron(II) chloride, oxalic acid, *N,N*-dimethylacetamide (DMA), sodium oxalate, hydrogen peroxide (H_2O_2), phenol, benzene, ethyl benzene, and trichloroethylene were purchased from Sigma-Aldrich Co. Ltd. All chemicals were of analytical grade and used without further purification.

3.2. Synthesis of the catalyst: A solution containing 1 mmol of oxalic acid and 10 mL of *N,N*-dimethylacetamide (DMA) was continuously stirred to form a homogeneous mixture. Then, 1 mmol of iron chloride tetrahydrate and 12 mL of deionized water were added into the solution. After stirring for 5 min, yellow colored precipitate was formed. After filtration and washing with deionized water and ethanol, respectively, the obtained solid was dried at 333 K under vacuum for 12 h ($\text{FeC}_2\text{O}_4 \cdot 2\text{H}_2\text{O}$). Micro-mesoporous iron(III) oxide (MMIO) was obtained by thermal decomposition of as-prepared $\text{FeC}_2\text{O}_4 \cdot 2\text{H}_2\text{O}$ in air. In a typical experiment, 1 g of the powdered precursor was spread on the bottom of a crucible in a thin layer (~1 mm thick) and heated in air at the conversion temperature of 448 K for 12 h.

3.3. Kinetic measurements of hydrogen peroxide decomposition: The catalytic activity of iron(III) oxide was performed based on our previous study.¹⁵ Briefly, a flask containing a mixture of 0.02 M hydrogen peroxide and the catalyst (1 g/L) was shaken to provide enough dispersion of the catalyst particles. The pH of the reaction mixture was not adjusted by buffer solution to avoid reaction of $\bullet\text{OH}$ with the buffer medium. The pH of the reaction mixture was observed to be 6.3-6.5. Samples of solution taken at different time intervals were filtered, and the hydrogen peroxide concentration was measured by the permanganate titration method.

3.4. Catalytic activity of MMIO in degradation of organic pollutants: In a typical experiment, phenol [100 ppm] and catalyst [200 mg/L] were mixed and sonicated to ensure the sufficient dispersion of the catalyst. This was followed by the drop-wise addition of the H_2O_2 (initial $[\text{H}_2\text{O}_2] = 530$ ppm), and was stirred for 30 min at 313 K. Subsequently, aliquots of 2 mL were taken and filtered through the filtration funnel (porosity 4). The degree of phenol conversion was monitored by an Agilent 6820 gas chromatograph. Similarly, organic molecules such as benzene, ethyl benzene, and trichloroethylene with initial concentrations of 100, 60, and 113 ppm, respectively, were chosen as substrates. Reaction conditions: initial $[\text{H}_2\text{O}_2] = 530$ ppm, $T = 313$ K, $\text{pH} = 6.7$, 200 mg/L of catalyst. The blank test without the use of MMIO catalyst (no degradation observed) was also conducted.

3.5. Characterization techniques

X-ray diffraction (XRD) patterns of all samples were recorded on a PANalytical X'Pert PRO diffractometer in Bragg-Bretano geometry with iron filtered Co K α radiation (40 kV, 30 mA) equipped with an Xcelerator detector and programmable divergence and diffracted beam anti scatter slits. ^{57}Fe Mössbauer spectrum were recorded with 1024 channels and measured at room temperature employing a MS2006 Mössbauer spectrometer based on virtual instrumentation technique, operating at a constant acceleration mode and equipped with a $^{57}\text{Co}(\text{Rh})$ source. Thermogravimetric analyses (TGA) of starting iron(II) oxalate precursor were performed in air atmosphere at a heating rate of 10 °C min $^{-1}$ using an STA 449 C Jupiter analyzer.

Field emission scanning electron microscopy (FESEM) images were taken on a Hitachi 6600 FEG microscope operating in the secondary electron mode and using an accelerating voltage of 5 kV. Transmission electron microscopy (TEM) investigations were performed at 80 kV accelerating voltage on FEI TitanG2 60-300 transmission electron microscope equipped with X-FEG electron gun, objective-lens image spherical aberration corrector and chemiSTEM EDS detector.

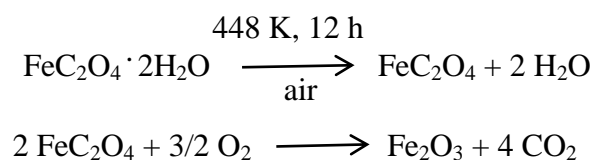
Nitrogen adsorption-desorption isotherms at 77 K were measured up to the saturation pressure of nitrogen and obtained by the static volumetric technique on an Autosorb-iQ-C analyzer (Quantachrome). The size of iron(III) oxide nanoparticles from pre-crushed iron(II) oxalate precursor was determined by a dynamic light scattering (DLS) using a Zetasizer Nano particle analyser ZEN3600 (Malvern Instruments, UK).

DMPO-trapped electron paramagnetic resonance (EPR) spectrum of prepared iron oxide-DMA was carried out to measure HO \cdot production in iron oxide/H $_2$ O $_2$ system. Spin-trapping was accomplished by spin-trap compound, DMPO (5,5-dimethyl-1-pyrroline N-oxide). The conversions of phenol, benzene, ethyl benzene, and trichloroethylene was monitored by a gas chromatography (GC Agilent 6820) equipped with a capillary column of Agilent DB-5 type under the operation parameters: inlet temperature of 300 °C, FID temperature of 300 °C, oven temperature ramp from 80 °C to 250 °C at a rate of 10 °C/min.

4. Overview of the main results of the thesis

4.1. Micro-mesoporous iron oxide (MMIO) in H₂O₂ decomposition and organic pollutant degradation

A simple two-step synthetic method is used to synthesize the iron oxide based Fenton nanocatalysts. This method is based on the direct precipitation of iron(II) oxalate precursor from an equimolar mixture of oxalic acid and Fe(II) chloride in DMA at room temperature (step 1), followed by solid-state isothermal treatment at 448 K for 12 h in air (step 2). The final iron oxide product (α -Fe₂O₃) is tagged as FIO throughout the text for clarity; detailed descriptions of these two synthetic steps are given in the experimental section.



Scheme 1: Two step decomposition of iron oxalate to form iron oxide

The FESEM images of the iron oxalate and the final FIO catalyst are shown in Fig. 1a and 1b, respectively. Interestingly, the FIO material preserved the complex 3D morphology (rods/flower-like) throughout synthesis, from precursor to product, despite the thermal process. Structurally, the 3D organization of the crystallites in FIO, likewise in the iron oxalate precursor is driven by the self-assembly process of micrometer-sized rods, which are further composed of nanosized particles (5-7 nm). These small nanoparticles represent therefore the building unit from which the 3D nanoarchitectures of FIO emerge (Fig. 1d). Clearly, the thermally induced solid-state decomposition of micrometer-sized flower-like iron(II) oxalate performed at the lowest possible conversion temperature resulted in a very slow evolution of gaseous products enabling the conservation of the original precursor morphology and the generation of a unique porous network of iron(III) oxide nanoparticles.

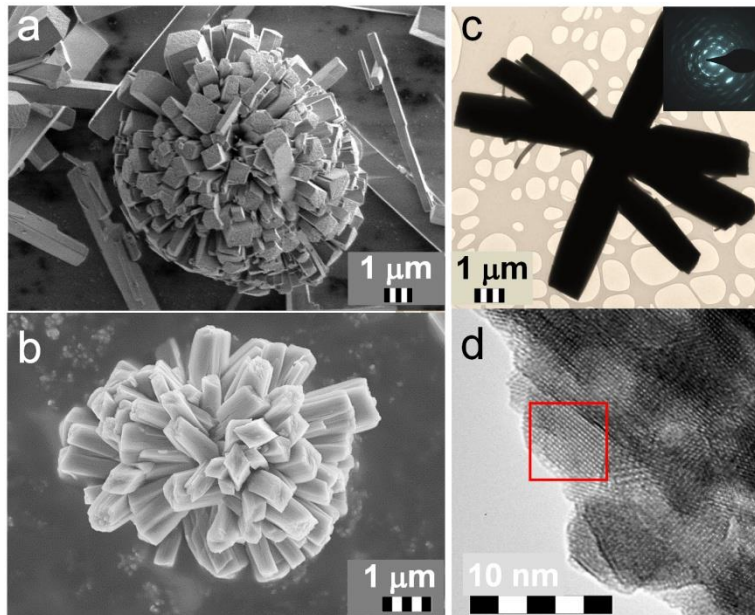


Figure 1: FESEM image of the a) iron(II)oxalate precursor and b) FIO, c) The TEM image of FIO. The inset depicts the SAED pattern and HRTEM image of d) FIO.

Furthermore, this procedure allowed to remove smoothly and completely the solvent molecules in the material, as validated by elemental (C 1.05 ± 0.02 %, N 0.06 ± 0.01 %, and H 1.475 ± 0.10 %) analysis of the FIO catalyst. This result highlights not only the complete conversion of iron(II) oxalate precursor to iron(III) oxide, but also the cleanness of the process that prevents contamination by solvent molecules. This method represents, in our opinion, an easier alternative with respect to more complex procedures that employ structure directing templates for attaining similar results.

The chemical composition, crystallinity and phase purity of FIO were studied by XRD analysis and complemented by Mössbauer spectroscopy (Figs. 2a and b). The XRD pattern of FIO features broad scattering line typical for ultra-small particles. The result is in accord with its 3D structural assembly depicted previously in the SEM and TEM micrographs (rods/flowers-like structures), as the bulk material is indeed formed by merging together small (5-7 nm) nanoparticles units. Overall, two main diffractions signals occurs from the XRD envelope ($2\theta = 39.7^\circ$ and 74.4°), with scattering-angle values that support the formation of pure hematite phase. Also the selected area electron diffraction (SAED) from TEM analysis (inset in Fig. 1c) gives a direct conformation of the polycrystalline nature of the material, with a pattern that is also fully consistent with the indexes expected for the hematite phase, $\alpha\text{-Fe}_2\text{O}_3$.

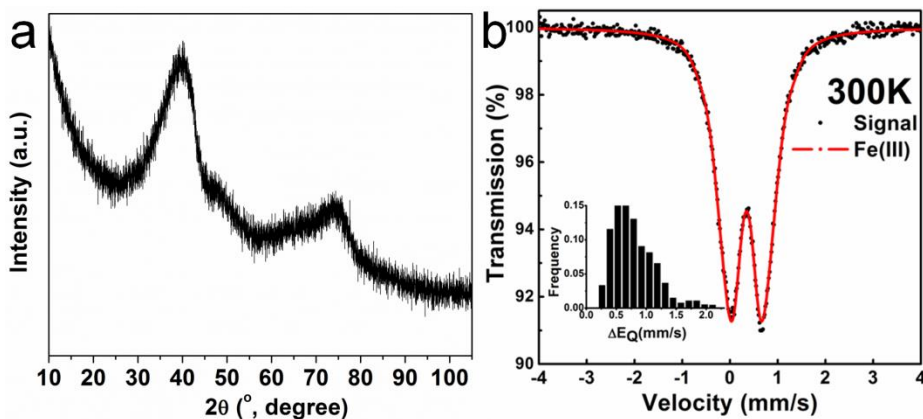


Figure 2: a) XRD pattern, b) room-temperature ^{57}Fe Mossbauer spectrum of the FIO catalyst evidencing the hematite structure.

Mössbauer measurement (Fig. 2b) of the FIO catalyst performed at room temperature shows the presence of one doublet, with an isomer shift (δ) of 0.37 ± 0.1 mm/s and a quadrupole splitting (ΔE_Q) of 0.80 ± 0.01 mm/s, values that signify high-spin ($S = 5/2$) iron Fe(III) in a superparamagnetic state, as expected to occur for nanometer sized hematite.³⁵ From these results we may conclude that the thermal treatment of oxalate precursor using simple solid-state synthesis performed at minimum decomposition temperature provides an easy access to ultra-small single-phase pure hematite nanoparticles and a means to preserve the 3D morphology encoded in the original precursor (iron oxalate).

The successful assembly of a heterogeneous Fenton catalyst requires that the interactions between reactant (H_2O_2) and available active Fe(III) centers and voids present on the catalyst's surface are maximized; hence and in the best possible scenario, the envisioned synthetic protocol should generate materials with optimized physical parameters such as surface area and porosity. The specific surface area (S_{BET}) and porosity (V_p) of FIO were evaluated experimentally by measuring the nitrogen adsorption-desorption isotherms.

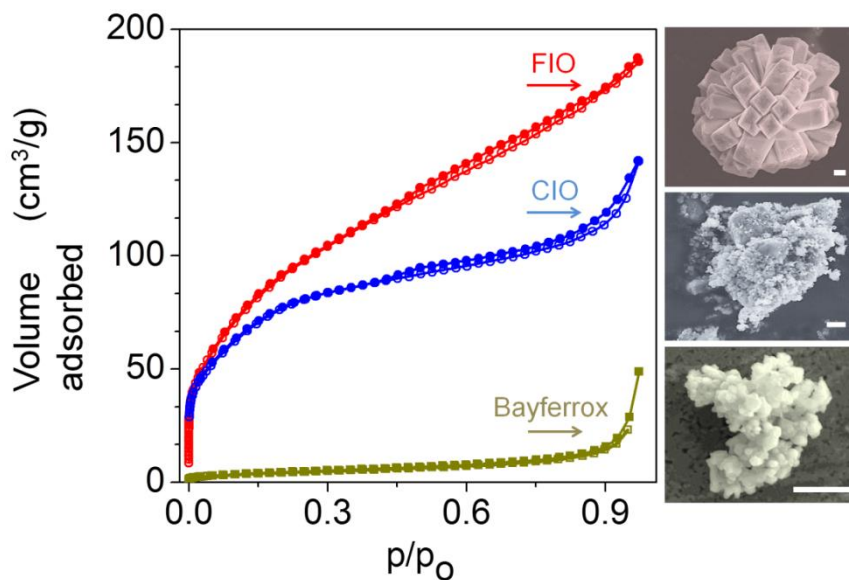


Figure 3: The nitrogen adsorption (open symbols)–desorption (closed symbols) isotherms of FIO (3D morphology) compared to the pre-crushed sample CIO and the commercially available hematite material (Bayferrox). The micrographs on the right are the corresponding SEM images. The size bars are equal to 0.5 μm .

Fig. 3 (red curve) shows the trends reported for FIO. Here, the N_2 adsorption-desorption isotherms behaviour can be dissected into combination of Type I (microporous structure) and Type IV (mesoporous structure) processes. In addition we can observe the emergence of a H4-type hysteresis loop, with the characteristic step-down behavior at relative pressures (p/p_0) near to 0.4. The attained S_{BET} value of FIO catalyst is large and reaches the value of $345 \text{ m}^2/\text{g}$ ($\pm 2\%$), with the pore volume (V_{p}) of 0.28 cc/g . The isotherms and type of hysteresis loop observed in FIO are typical of micro-mesoporous materials having a complex pore-network, along with bottleneck type pores. In contrast, the commercially available iron oxide, sold as Bayferrox, whose nitrogen adsorption-desorption isotherms are comprised in Fig. 3 (green curve) for comparison, shows a much lower surface area ($\sim 15 \text{ m}^2/\text{g}$) and significantly smaller pore volume of 0.03 cc/g .

The effective catalytic ability of FIO to promote H_2O_2 decomposition was probed via permanganate titration, using the heterogeneous admixture of the two components ($0.02 \text{ M H}_2\text{O}_2$ and 1 g/L of FIO catalyst, pH 6.3-6.5) at room temperature.

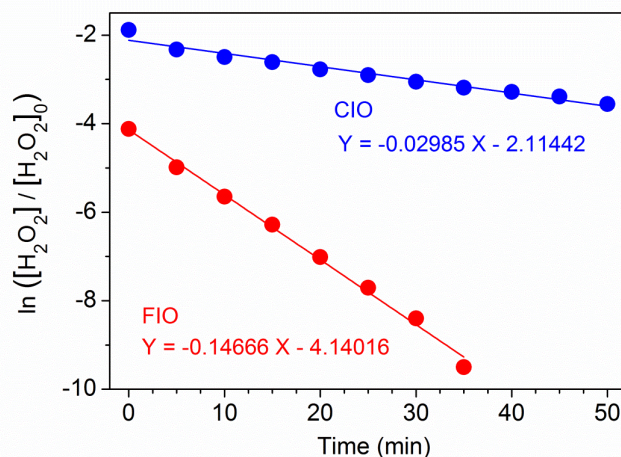


Figure 4: Kinetic measurements of hydrogen peroxide decomposition catalyzed by FIO (red circles) and CIO (blue circles).

We used the permanganate titration method in order to evaluate the kinetic parameters (Experimental details). The methodology consists of measuring the unreacted amount of peroxide left in solution, from a series of aliquots of the iron oxide/H₂O₂ admixture taken at different time intervals. The observed rate of H₂O₂ decomposition (k_1) followed the first-order kinetics, and topped the record value of $1.43 \times 10^{-1} \text{ min}^{-1}$ ($R^2 > 0.999$, fig.4) with a specific rate constant ($K_{sp} = k_1/S_{BET}$) of $0.414 \times 10^{-3} \text{ g min}^{-1} \text{ m}^{-2}$. To the best of our knowledge, this is the highest rate constants of H₂O₂ decomposition available today for any iron oxide based Fenton catalyst. This value is one order of magnitude larger compared to those reported for similar oxalate-derived hematite systems. It is important to highlight that our previously reported Fenton catalyst (hematite-based), which lacks a specific 3D morphology, but still scored one of the highest value for the H₂O₂ decomposition ($2.2 \times 10^{-2} \text{ min}^{-1}$); yet, even this catalyst is by far less efficient than FIO, even though it has the similar surface area ($337 \text{ m}^2/\text{g}$) of FIO. Hence, we speculate that such structural organization and self-assembly of ultra-small iron oxide nanoparticles into organized 3D architectures has a direct impact on the material's catalytic activity in the H₂O₂ decomposition rate.

To prove this hypothesis, we altered the 3D morphology of FIO. Firstly, we took the intact iron oxalate precursor (i.e., the product from step 1 in the synthesis) with its 3D organization, and then mechanically crushed the material in a way to destroy thoroughly the rod/flower-like 3D architectures.

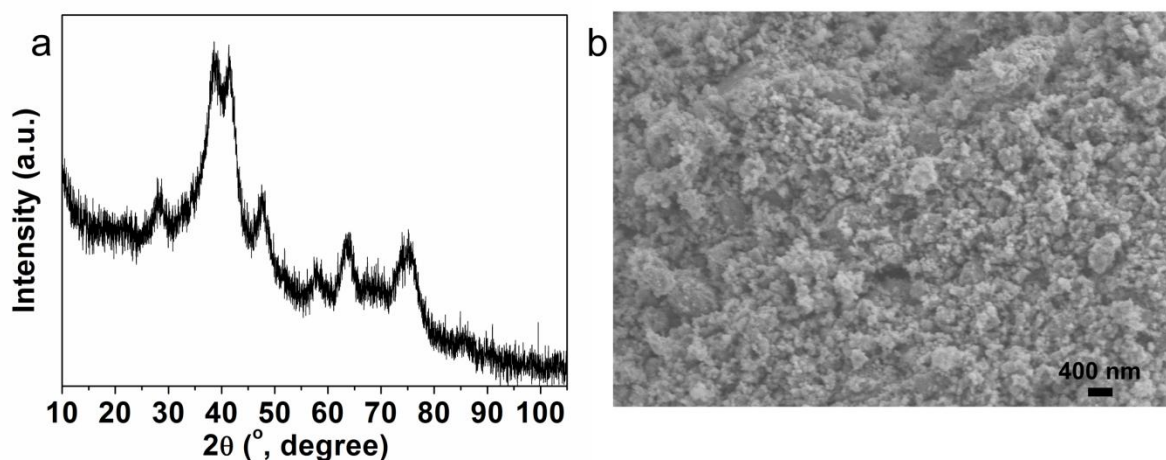


Figure 5: a) XRD pattern and b) FESEM image of the CIO sample.

After keeping the following heating procedure unchanged (namely, leaving the entire synthetic procedure unchanged), the morphology and catalytic proclivity of the so-formed hematite catalyst was finally tested. As expected, the crushed oxalate precursor lacks such 3D organized structures (rod/flower-like morphology), after the thermal treatment, (Fig. 5b). This material, labelled thereafter as CIO, still keeps the single-phase hematite structure but it encodes a higher degree of crystallinity, due to the better evolution of gases occurring within the calcination process (Fig 5a).

The surface and catalytic properties of CIO (N_2 adsorption-desorption, H_2O_2 activation) were then measured and evaluated with those encoded in FIO, in order to assess the importance of the morphological variable in the decomposition rate of hydrogen peroxide (see the comparisons in Fig 3 and 4). The catalytic activity of CIO, expressed as a rate of H_2O_2 decomposition, decreased by one order of magnitude (k_1 of $0.29 \times 10^{-1} \text{ min}^{-1}$; see fig 4; $K_{sp} = 0.1 \times 10^{-3} \text{ g min}^{-1} \text{ m}^{-2}$).

The suppressed activity of CIO is due to a loss of the micro-mesoporous structure of the catalyst (Fig. 5b), as also confirmed from the material's lower specific surface area ($290 \text{ m}^2/\text{g}$) and pore volume (V_p , 0.19 cc/g) in accordance to BET measurements (Fig. 3 blue curve). Another factor that seems to contribute to the witnessed differences in catalytic ability between FIO and CIO can be associated with their different number of exposed facets to the bulk.

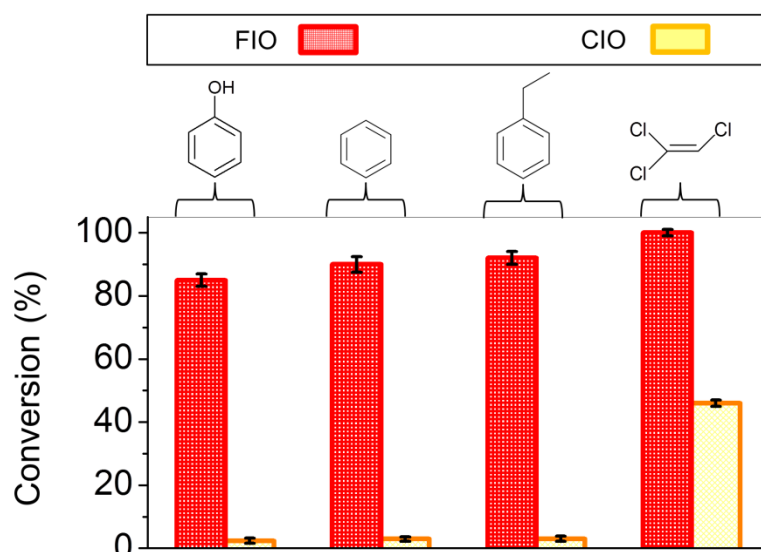


Figure 6: The catalytic degradation of aromatic and chlorinated pollutants (60–113 ppm) promoted by FIO/and CIO/H₂O₂ in water expressed as percentage (%).

The higher catalytic efficiency of FIO towards H₂O₂ decomposition may mirror in fact a higher number of active iron (III) sites; these active centres may continue to remain accessible during turn-over, due to the rigid 3D architecture. On the contrary, in CIO there is a lack of rigidity in the micro-arrangement, since the material is composed of individual nanoparticles simply aggregated together. As such, this factor may produce less organized and less easily accessible sites, which are in turn not able to promote the H₂O₂ activation as effectively.

The presence of the micro-mesoporous 3D nanoarchitecture in the FIO catalysts and, on the contrary, its absence in the CIO material stands up as one of the main factor that drives high degradation capability of FIO against various organic pollutants.

Fig. 6 shows the efficacy of FIO in the remediation of toxic organic molecules such as phenol, benzene, ethylbenzene, and trichloroethylene as contained in model systems of polluted water compared to CIO (experimental details). Here, the micro-mesoporous iron oxide serves as an active catalyst in the generation of hydroxyl radical (\bullet OH) from H₂O₂, a reactive specie that attacks the aromatic ring of benzene, ethyl benzene, and phenol for their degradation. The degradation of trichloroethylene follows a different pathway, and can be depicted as an oxidative dechlorination reaction.^{22,35-37} Fig. 6 shows the efficiency of FIO to degrade the pollutants compared to CIO, reaching percentages of pollutant conversion of 85-100% in just 30 minutes. The ability of CIO to degrade the studied organic pollutants is very small, with conversions ranging from 2% to 46%. It is worth emphasizing that such activity loss is not due to the failure

of ClO to promote generation of $\cdot\text{OH}/\cdot\text{OOH}$ radical species, as proven by electron paramagnetic resonance (EPR) spectroscopy (Fig. 7), but rather to the material's lower proclivity to perform an effective coupling of H_2O_2 activation with the pollutant degradation. Generation of $\cdot\text{OH}/\cdot\text{OOH}$ in solution has been confirmed by monitoring the process of H_2O_2 activation in presence of FIO and ClO through spin trapping technique, using DMPO (5,5-dimethyl-1-pyrroline *N*-oxide) as trapping agent, and with the help of EPR spectroscopy.

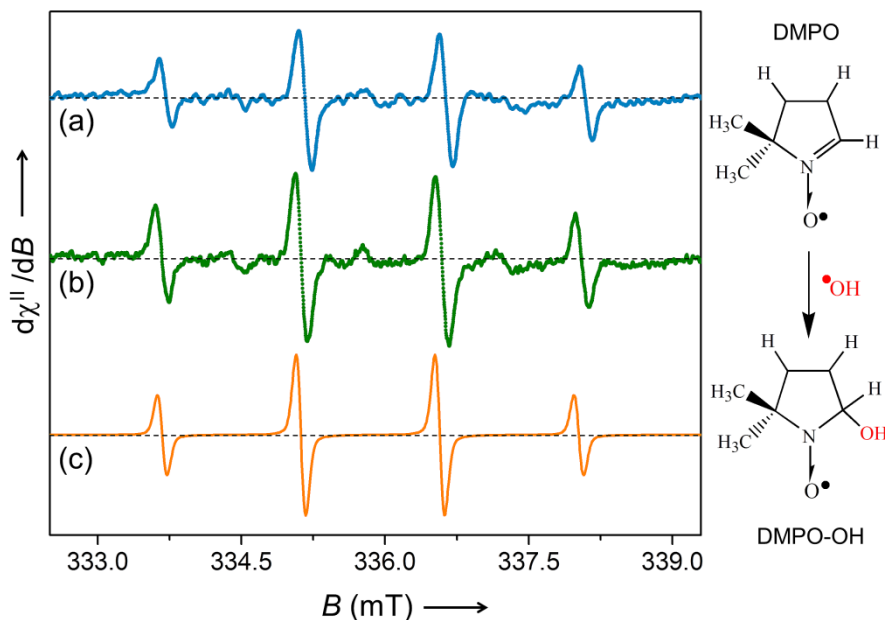


Figure 7: Left side: X-band (9.4 GHz) EPR spectra of the DMPO–OH radical adduct as obtained at room temperature in fluid solutions within the remediation process (catalyst/ H_2O_2 /organic pollutant): (a) DMPO–OH signal from a mixture of the ClO sample, H_2O_2 and benzene; (b) DMPO–OH signal from a mixture of FIO, H_2O_2 and benzene; and (c) EPR computer simulation of the DMPO–OH signal (a_N of 1.45 mT and a_H of 1.45 mT, $g_{iso} \approx 2.006$, and the Lorentzian/Gaussian-line ratio of 0.5). Right side: Spin trapping process of the hydroxyl radical by the DMPO molecule and the formation of DMPO–OH.

Fig. 7 shows the characteristic EPR envelopes obtained in solution where the formation of DMPO-OH radical adduct is highlighted. The DMPO-OH spin active molecule result from trapping the $\cdot\text{OH}/\cdot\text{OOH}$ radicals generated during the remediation process (catalyst/ H_2O_2 /pollutant). In particular, Fig. 7a displays the DMPO-OH signal obtained from the heterogeneous mixture of ClO/ H_2O_2 /benzene and Fig. 7b the same radical signal obtained from the mixture of FIO/ H_2O_2 /benzene. For comparison, Fig. 7c shows the simulated EPR signal of the DMPO-OH radical adduct. Thus, the 3D structural organization of the nanoparticles (the

presence of micro-mesoporous structure) in FIO plays a pivotal role in driving to excellence the remediation process. This phenomenon has been termed as morphology-dependent nanocatalysis, due to the selective exposure of specific crystal facets^{38,39} which is similar for FIO.

A novel methodology for the synthesis of highly organized MMIO catalysts with encoded 3D arrangement and extraordinary catalytic efficiency is described. This precursor-based synthetic pathway allowed the successful assembly of a 3D rod/flower-like Fenton catalyst that exhibited the highest activity known for the H₂O₂ decomposition, a process that is employed here for the fast remediation of contaminated water with organic pollutants. At the same time, it has been established that this superior efficiency of remediation is lost when the catalyst 3D morphology is not present. Finally, in addition to the well-known variables such as chemical composition, size, surface area, pore volume, crystal structure, and crystallinity of the catalyst, the morphological feature (3D assembly of nanoparticles) is found to play a major role in the materials' catalytic activity toward H₂O₂ decomposition, and thereby the material's ability to remediate water solutions from various organic pollutants.

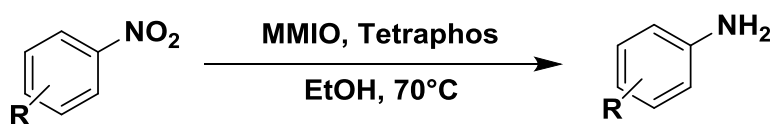
4.2. MMIO as catalyst for base free transfer hydrogenation of nitroarenes

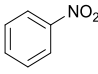
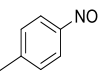
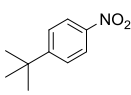
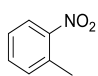
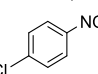
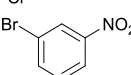
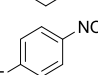
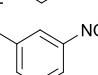
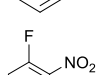
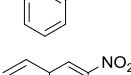
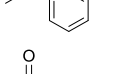
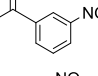
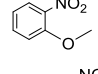
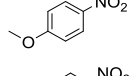
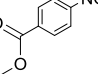
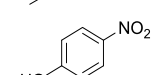
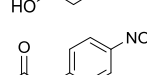
In the present study, we describe efficient and useful protocol for the transfer hydrogenation of nitroarenes employing a flower/rod-shaped MMIO⁴⁰ with formic acid as the reducing agent in presence of ligand, tris[(2-diphenyl-ethyl)phosphine] under base-free conditions (yield up to 98%). The as-synthesized MMIO catalyst is characterized by several techniques namely, FE-SEM, HRTEM, N₂-adsorption-desorption isotherm and Mössbauer spectroscopy. The salient features of this protocol are the usage of formic acid as a reducing agent and the reusability of the catalyst in the absence of additional base. In contrast to other catalysts examined, only MMIO exhibited excellent conversion and yield (95%) while commercial iron (III) oxide afforded 60% yield. We believe that the present work will motivate the use of MMIO for other promising organic reactions.

To optimize the reaction conditions, the reduction of 4-nitroanisole was studied as a model substrate using MMIO as catalyst, formic acid as hydrogen source, tetrachos as ligand and ethanol as solvent at 70 °C for 40 min. The impact of various reaction parameters has been explored on the model reaction such as catalyst screening, influence of ligands, effect of solvent, catalyst loading, effect of hydrogen donor, reaction time and temperature.

After the optimized conditions were established, we have extended our protocol for transfer hydrogenation of wide range of aromatic nitro compounds with diverse substituent groups (Table 1). Various alkyl substituted aromatic nitroarenes are reduced to afford the corresponding anilines in good conversion and moderate yield without forming any side products such as hydroxylamines, hydrazines, azoarenes, or azoxyarenes (Table 1, entries 2-4). The reduction of halogen substituted (4-chloro-, 3-bromo-, 4-fluoro-, and 3-iodo-) nitrobenzenes was completed within 40 minutes and the amines were obtained in high yields (Table 1, entries 5-8). The reduction of 2-fluoronitrobenzene required little longer time and no dehalogenation processes was observed for any substrates (Table 1, entry 9). In the case of *m*-nitrostyrene, it reduced to aniline in excellent yield (98%) (Table 1, entry 10). Further, various industrially important aromatic nitro substrates containing other functional groups such as ketone, ether, methoxy, ester, and hydroxy were successfully reduced easily into corresponding amines in excellent yields (Table 1, entries 11-16). In addition, reduction of heterocyclic nitroarene was also tested, giving the corresponding product in 85% yield (Table 1, entry 17). Interestingly, the present catalytic system is very selective towards nitro group reduction retaining other reducible functional groups.

Table 1: MMIO catalyzed reduction of nitroarenes.



Entry	Substrate	Time	Conversion (%) ^b	Yield (%) ^b
1		40	>99	84
2		50	>99	83
3		60	>99	62
4		40	>99	85
5		40	>99	75
6		40	>99	87
7		40	>99	83
8		40	>99	85
9		50	>99	80
10		40	>99	98
11		40	>99	82
12		40	>99	98
13		40	>99	95
14		40	>99	84
15		40	>99	85
16		40	>99	91
17		40	>99	85

^aReaction conditions - Nitroarene (0.27 mmol), HCOOH (2.7 mmol), Catalyst (20 mg), tetraphos (6 mol%), ethanol (2 mL), Temp. 70 °C, 40 min. ^bDetermined by GC using n-hexadecane as internal standard.

Catalyst activity and stability are main requirements to a highly active heterogeneous catalyst. To that end, we tested the recyclability of MMIO for selective transfer hydrogenation of 4-nitroanisole. MMIO catalyst was separated by filtration method after the completion of reaction. The filtrate catalyst was washed with distilled water for five times and methanol to remove the remaining organic compounds. Then it was dried in oven and reused for next run. The MMIO catalyst was found to be successfully active when recycled up to four consecutive cycles.

In conclusion, we present an efficient and practical protocol for the preparation of heterogeneous MMIO catalyst, prepared by the solid state thermal treatment of iron oxalate precursors. This MMIO catalyst was tested for base-free reduction of nitroarenes to obtain their corresponding products in good to excellent yield. The main advantage of catalyst is that it is robust, and it can be prepared from inexpensive raw materials. We believe that the combination of MMIO and tetraphos-based ligands could be employed for several other industrially important transfer hydrogenation reactions.

4.3. Porous magnetite prepared from MMIO and used for the reduction of nitroarenes

Herein, we report an easy approach for the synthesis of porous magnetite, through a template free thermal decomposition method to produce hematite followed by its reduction using hydrogen gas. It is very interesting to note that the flower/rod like morphology of the precursor is well preserved even after the hydrogen treatment. The as-prepared porous magnetite catalyst is characterized by several techniques namely, XRD, FESEM, TEM, N₂-adsorption-desorption isotherm and Mössbauer spectroscopy. The porous magnetite acts as a catalyst for the transfer hydrogenation of nitroarenes with hydrazine hydrate as the reducing agent in a small scale microwave batch heating device (yield up to 98%). The salient features of this work are the usage of microwave technology for the reduction of nitroarenes (porous magnetite as a catalyst) using hydrazine hydrate as a reducing agent and the excellent reusability of catalyst.

Magnetite can be prepared by the reduction of hematite under H₂ atmosphere as reported by several groups. In the present work we performed two step approaches to prepare porous magnetite. Firstly, thermally induced solid state reaction was used to prepare porous hematite, followed by reduction in hydrogen atmosphere to yield magnetite. The stepwise transformation of hematite to magnetite via hydrogen reduction process was *in-situ* monitored by XRD. At 220 °C, the diffraction lines corresponding to face-centered cubic (*fcc*) structure of

magnetite/maghemite start to occur and their intensities gradually increase during 1 h of isothermal treatment. Therefore we choose temperature 220 °C for 2 h as the optimal condition for the preparation of porous magnetite form iron (III) oxide particles using a tube furnace under hydrogen atmosphere.

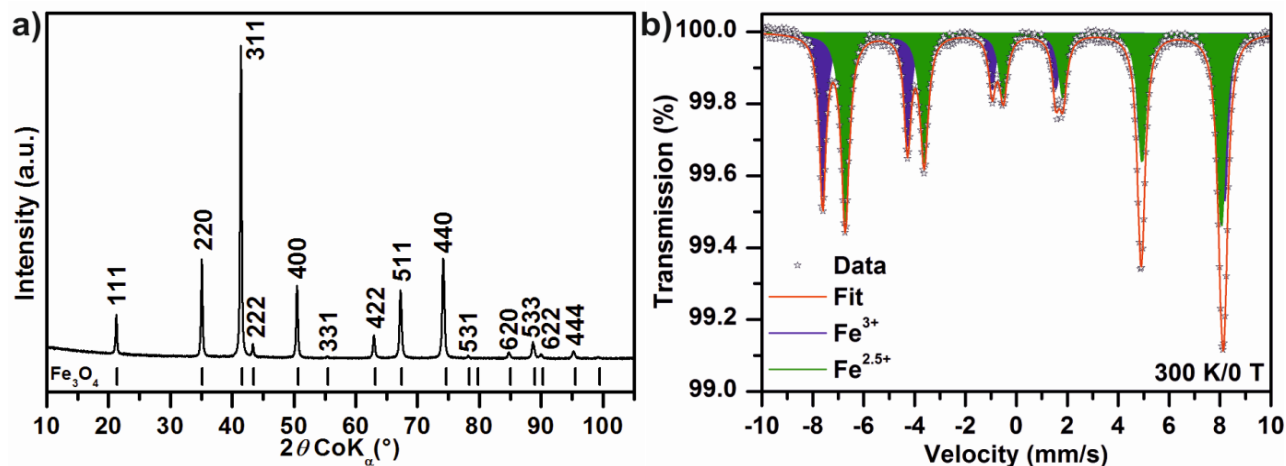


Figure 8: a) XRD pattern and b) Mössbauer spectra of porous magnetite.

Fig. 8a represent XRD pattern of porous magnetite sample. All of the diffraction lines can be clearly ascribed to standard *fcc* structure of Fe_3O_4 (space group: $Fd3m$ (227), JCPDS card No. 01-089-3854). Although the isostructural character of maghemite and magnetite causes difficulties in direct and precise identification of these phases by XRD point of view, the cell parameter indicates correct suggestion. The cell parameter varies from 0.8351 nm for maghemite and 0.8396 nm for stoichiometric magnetite.^{41,42} The cell parameter of cubic structure in prepared sample is 0.8394 nm which is in very good agreement with values described in literature for magnetite. No evidence of impurities can be found in the XRD pattern. Nevertheless, the Mössbauer spectroscopy is the very powerful experimental technique which provides precise identification of valence state of iron atoms and cations distribution and more generally, identification of iron compounds.

Therefore, Mössbauer spectroscopy was employed for direct identification of iron oxide form (Fig. 8b). The obtained spectrum consists of two magnetically split subspectra (i.e., sextets). First of them, with hyperfine parameters $\delta = 0.27 \text{ mm s}^{-1}$, $\varepsilon_Q = -0.01 \text{ mm s}^{-1}$, $B_{hf} = 49.0 \text{ T}$, and line width $\Gamma = 0.33 \text{ mm s}^{-1}$, which are typical for Fe^{3+} ions in tetrahedral sites in magnetite; and second subspectrum, with $\delta = 0.67 \text{ mm s}^{-1}$, $\varepsilon_Q = 0.00 \text{ mm s}^{-1}$, $B_{hf} = 46.0 \text{ T}$, and line width

$\Gamma = 0.39 \text{ mm s}^{-1}$, which corresponds to octahedral sites in magnetite structure occupied by Fe^{2+} and Fe^{3+} . The occurrence of only sextet for both Fe^{2+} and Fe^{3+} in octahedral sites is caused by electron hopping effect, which is slightly faster than characteristic time of Mossbauer detection.⁴³ Relative areas of tetrahedral and octahedral subspectra are 41 and 59 %, respectively. This difference from ideal spectral area of 33 and 67 % for stoichiometric magnetite indicates slight nonstoichiometry in magnetite. Unpaired Fe^{3+} ions in octahedral sites which do not participate in electron hopping process create their own subspectrum with hyperfine parameters overlapping with these for subspectrum representing Fe^{3+} in tetrahedral sites. Therefore these two subspectra with overlapping parameters are fitted as one and its relative area is increased to the detriment of subspectra representing mixed valence $\text{Fe}^{2.5+}$ in octahedral sites.

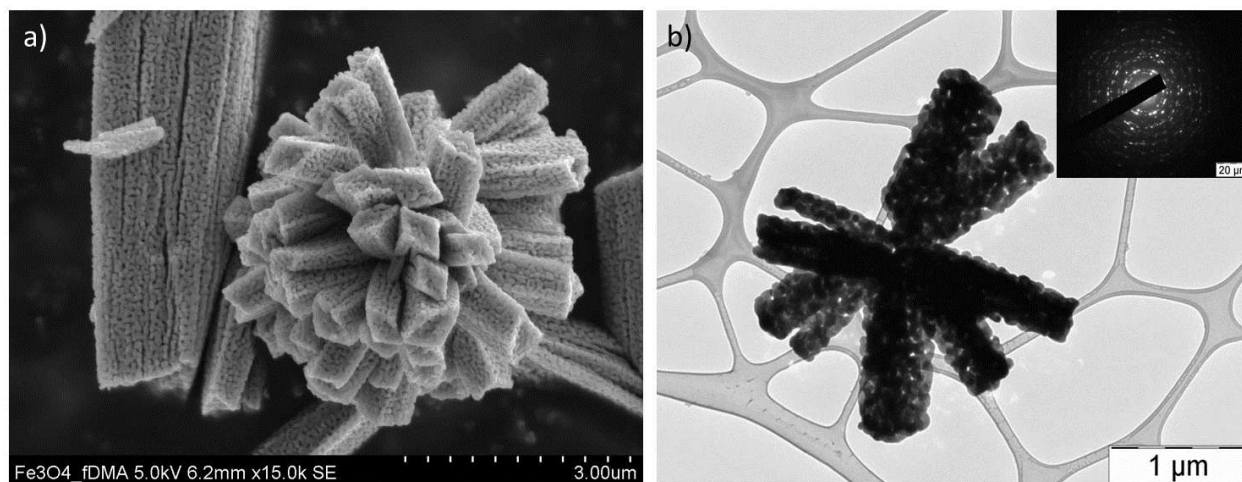


Figure 9: a) SEM and b) TEM image of porous magnetite, inset showing corresponding SAED pattern.

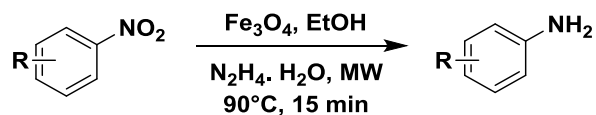
The morphology of the prepared samples was obtained using SEM and TEM. The SEM image (Fig. 9a) of porous magnetite revealed the retention of rod/flower like pattern as found in the case of hematite. From the TEM image (Fig. 9b), it can be seen that the individual nanorods possess an average size 300 nm and the self-assembled floral pattern have diameter in the range of 3 micro meters.

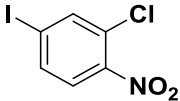
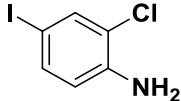
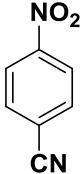
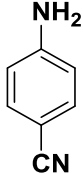
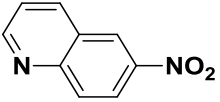
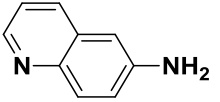
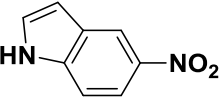
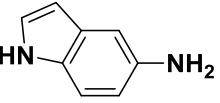
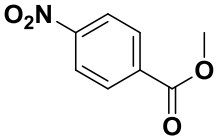
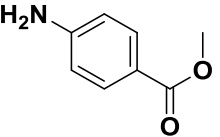
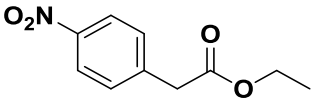
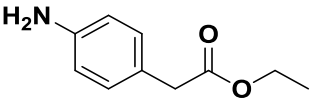
The inset in Fig. 9b shows the electron diffraction pattern of the particles that are polycrystalline in nature. The width of the nanorods forming rod/flower like pattern was found to be uniform along its entire length as evidenced from the TEM image. The pores might be formed during recrystallization process or from the elimination of water during the reduction process. The N_2

adsorption–desorption isotherms show Type II isotherm for the magnetite with no significant hysteresis. The specific surface area obtained from BET method is 20 m²/g.

Furthermore, to examine the efficiency of the catalyst we tested the reduction reaction. To optimize the reaction we used nitrobenzene as a model substrate using magnetite as catalyst, hydrazine hydrate as hydrogen donor and ethanol as solvent at 90 °C for 15 min in microwave reactor.

Table 2: Catalytic reduction of nitro compounds^a



Entry	Nitro compound	Products	^a Conversion	^b Yield %
1			>99	96
2			>99	96
3			>99	95
4			>96	92 ^c
5			>97	96
6			93	92

7			>42	37 ^c
8			>99	98
9			>97	94 ^c
10			99	96 ^d
11			99	96
12			99	96
13			99	96 ^e
14			99	95 ^f
15			99	95 ^e

^a**Reaction condition:** Nitrobenzene (0.5 mmol), Hydrazine hydrate (100 μ L), Fe_3O_4 (30 mg), EtOH (1.5 mL) Temp. 90°C, 15 min. ^bDetermined by GC using dodecane as an internal standard. ^creaction time 25 min. ^dreaction time 20 min. ^ereaction time 22 min. ^fisolated yield.

The optimized reaction conditions were then applied for varieties of nitro substrates with additional reducible group, electron donating and withdrawing group on benzene ring to check

the chemo selectivity of the catalyst. The results are summarized in Table 2. In most of the cases >99 % conversion and quantitative yield (calculated by GC) were obtained within 15 min at 90°C and only 4-nitrobenzamide showed 42% conversion (Table 2, entry 7). It is might be polar nature of the amidic compound. It has been observed that 6-nitro-2,3-dihydrobenzo[1,4]dioxine, 5-nitro-1H-indole and sterically hindered 1-methyl-2-nitrobenzene were completed in 25 min (Table 2, entries 15, 4 and 9), while 3-fluoro nitrobenzene and 4-methoxy nitrobenzene showed 99% conversion in 22 min (Table 2, entries 10 and 13). Interestingly, halogenated nitroarenes such as 2-chloro-4-iodo-1-nitrobenzene, 3-fluoro nitrobenzene, 4-bromo nitrobenzene, 4-chloro nitrobenzene showed the excellent conversion (Table 2, entries 1, 10, 11 and 12) without any de-halogenated product and also easily reducible ester group is tolerate with this catalytic system (Table 2, entries 5, 6). In additionally this catalytic system is very useful for the reduction of methyl (4-nitrophenyl)sulfane and selectively reduce 4-nitrobenzonitrile to 4-amino benzonitrile with excellent yield (>95%) and heterocyclic moiety (Table 2, entries 2, 8, 3 and 4). The synthesized magnetite was recycled and reused 10 times without any reactivation.

5. Summary

In conclusion, a novel methodology for the synthesis of highly organized micro-mesoporous iron(III) oxide catalysts with encoded 3D arrangement and extraordinary catalytic efficiency is described. This precursor-based synthetic pathway allowed the successful assembly of a 3D rod/flower-like Fenton catalyst that exhibited the highest activity known for the H₂O₂ decomposition, a process that is employed here for the fast remediation of contaminated water with organic pollutants. At the same time, it has been established that this superior efficiency of remediation is lost when the catalyst 3D morphology is not present. Finally, in addition to the well-known variables such as chemical composition, size, surface area, pore volume, crystal structure, and crystallinity of the catalyst, the morphological feature (3D assembly of nanoparticles) is found to play a major role in the materials' catalytic activity toward H₂O₂ decomposition, and thereby the material's ability to remediate water solutions from various organic pollutants.

This MMIO catalyst was also investigated for efficient reduction of nitroarenes to obtain their corresponding product in good to excellent yield under base-free conditions. The main advantage of MMIO is that it is robust, and it can be prepared from inexpensive raw materials. We believe that the combination of MMIO catalyst and tetraphos-based ligands could be employed for

several other industrially important transfer hydrogenation reactions. Also this MMIO catalyst was utilized for the synthesis of porous magnetite under hydrogen atmosphere and was utilized for the reduction of nitroarenes, which is suitable for industrially important and challenging substrates with other sensitive functional groups. A diverse range of anilines was obtained in excellent yields under the microwave conditions at 90 °C by using hydrazine hydrate as hydrogen source within 15 min that eliminates the use of a precious metal catalyst and hydrogen gas in the preparation of anilines. The porous magnetite prepared by this method was found to be very stable and used ten times successfully with minor decrease in its catalytic activity. Furthermore, the use of this catalyst is also safe and environmentally well suited. The excellent catalytic performance, simple procedure, easy separation, and the ability to recycle make this catalytic system impressive and useful alternative to other catalytic system.

6. References

- (1) Malaj, E.; von der Ohe, P. C.; Grote, M.; Kuhne, R.; Mondy, C. P.; Usseglio-Polatera, P.; Brack, W.; Schafer, R. B. *Proc. Natl. Acad. Sci. U.S.A.* **2014**, *111*, 9549.
- (2) Schwarzenbach, R. P.; Escher, B. I.; Fenner, K.; Hofstetter, T. B.; Johnson, C. A.; von Gunten, U.; Wehrli, B. *Science* **2006**, *313*, 1072.
- (3) Shannon, M. A.; Bohn, P. W.; Elimelech, M.; Georgiadis, J. G.; Marinas, B. J.; Mayes, A. M. *Nature* **2008**, *452*, 301.
- (4) Yang, X. J.; Xu, X. M.; Xu, J.; Han, Y. F. *J. Am. Chem. Soc.* **2013**, *135*, 16058.
- (5) Zhang, M. L.; Yao, Q. F.; Guan, W. J.; Lu, C.; Lin, J. M. *J. Phys. Chem. C* **2014**, *118*, 10441.
- (6) Brillas, E.; Sires, I.; Oturan, M. A. *Chem. Rev.* **2009**, *109*, 6570.
- (7) Pignatello, J. J.; Oliveros, E.; MacKay, A. *Crit. Rev. Env. Sci. Tec.* **2006**, *36*, 1.
- (8) Dhakshinamoorthy, A.; Navalon, S.; Alvaro, M.; Garcia, H. *ChemSuschem* **2012**, *5*, 46.
- (9) Lu, A. H.; Salabas, E. L.; Schuth, F. *Angew. Chem. Int. Edit.* **2007**, *46*, 1222.
- (10) Perez, J. M. *Nat. Nanotechnol.* **2007**, *2*, 535.
- (11) Tartaj, P.; Morales, M. P.; Gonzalez-Carreno, T.; Veintemillas-Verdaguer, S.; Serna, C. J. *Adv. Mater.* **2011**, *23*, 5243.

- (12) Enami, S.; Sakamoto, Y.; Colussi, A. J. *Proc. Natl. Acad. Sci. U.S.A.* **2014**, *111*, 623.
- (13) Abbot, J.; Brown, D. G. *Int. J. Chem. Kinet.* **1990**, *22*, 963.
- (14) Chou, S. S.; Huang, C. P. *Appl. Catal. A-Gen.* **1999**, *185*, 237.
- (15) Hermanek, M.; Zboril, R.; Medrik, N.; Pechousek, J.; Gregor, C. *J. Am. Chem. Soc.* **2007**, *129*, 10929.
- (16) Hsieh, S. C.; Lin, P. Y. *J. Nanopart. Res.* **2012**, *14*.
- (17) Huang, C. P.; Huang, Y. H. *Appl. Catal. A-Gen.* **2008**, *346*, 140.
- (18) Huang, H. H.; Lu, M. C.; Chen, J. N. *Water Res.* **2001**, *35*, 2291.
- (19) Lin, S. S.; Gurol, M. D. *Environ. Sci. Technol.* **1998**, *32*, 1417.
- (20) Moura, F. C. C.; Araujo, M. H.; Costa, R. C. C.; Fabris, J. D.; Ardisson, J. D.; Macedo, W. A. A.; Lago, R. M. *Chemosphere* **2005**, *60*, 1118.
- (21) Valentine, R. L.; Wang, H. C. A. *J. Environ. Eng-Asce.* **1998**, *124*, 31.
- (22) Hartmann, M.; Kullmann, S.; Keller, H. *J. Mater. Chem.* **2010**, *20*, 9002.
- (23) Bautista, P.; Mohedano, A. F.; Casas, J. A.; Zazo, J. A.; Rodriguez, J. J. *J. of Chem. Technol. Biotechnol.* **2008**, *83*, 1323.
- (24) Jiao, F.; Bruce, P. G. *Angew. Chem. Int. Edit.* **2004**, *43*, 5958.
- (25) Jiao, F.; Jumas, J. C.; Womes, M.; Chadwick, A. V.; Harrison, A.; Bruce, P. G. *J. Am. Chem. Soc.* **2006**, *128*, 12905.
- (26) Ren, Y.; Ma, Z.; Bruce, P. G. *Chem. Soc. Rev.* **2012**, *41*, 4909.
- (27) Tiemann, M. *Chem. Mater.* **2008**, *20*, 961.
- (28) Liu, J.; Qiao, S. Z.; Hu, Q. H.; Lu, G. Q. *Small* **2011**, *7*, 425.
- (29) Yue, W. B.; Zhou, W. Z. *Prog. Nat. Sci.* **2008**, *18*, 1329.
- (30) Guo, L. M.; Arafune, H.; Teramae, N. *Langmuir* **2013**, *29*, 4404.
- (31) Yu, C. C.; Dong, X. P.; Guo, L. M.; Li, J. T.; Qin, F.; Zhang, L. X.; Shi, J. L.; Yan, D. S. *J. Phys. Chem. C.* **2008**, *112*, 13378.
- (32) Gregor, C.; Hermanek, M.; Jancik, D.; Pechousek, J.; Filip, J.; Hrbac, J.; Zboril, R. *Eur J. Inorg. Chem.* **2010**, 2343.
- (33) Hermanek, M.; Zboril, R.; Mashlan, M.; Machala, L.; Schneeweiss, O. *J. Mater. Chem.* **2006**, *16*, 1273.
- (34) Hermankova, P.; Hermanek, M.; Zboril, R. *Eur. J. Inorg. Chem.* **2010**, 1110.

- (35) Neyens, E.; Baeyens, J. *J. Hazard. Mater.* **2003**, *98*, 33.
- (36) Bautista, P.; Mohedano, A. F.; Casas, J. A.; Zazo, J. A.; Rodriguez, J. J. *J. Chem. Technol. Biot.* **2008**, *83*, 1323.
- (37) Gui, M. H.; Smuleac, V.; Ormsbee, L. E.; Sedlak, D. L.; Bhattacharyya, D. *J. Nanopart. Res.* **2012**, *14*.
- (38) Li, Y.; Shen, W. *J. Chem. Soc. Rev.* **2014**, *43*, 1543.
- (39) Xie, X. W.; Li, Y.; Liu, Z. Q.; Haruta, M.; Shen, W. *J. Nature* **2009**, *458*, 746.
- (40) Datta, K. J.; Gawande, M. B.; Datta, K. K. R.; Ranc, V.; Pechousek, J.; Krizek, M.; Tucek, J.; Kale, R.; Pospisil, P.; Varma, R. S.; Asefa, T.; Zoppellaro, G.; Zboril, R. *J. Mater. Chem. A* **2016**, *4*, 596.
- (41) Machala, L.; Tucek, J.; Zboril, R. *Chem. Mater.* **2011**, *23*, 3255.
- (42) Hai, H. T.; Kura, H.; Takahashi, M.; Ogawa, T. *J. Colloid. Interf. Sci.* **2010**, *341*, 194.
- (43) Doriguetto, A. C.; Fernandes, N. G.; Persiano, A. I. C.; Nunes, E.; Greneche, J. M.; Fabris, J. D. *Phys. Chem. Miner.* **2003**, *30*, 249.